X-ray Computed Tomography of Flame Structure in Porous Media Burners

Meng Wu, Jared Dunnmon, Yan Xia, Waldo Hinshaw, Norbert Pelc, Andreas Maier, Rebecca Fahrig, and Matthias Ihme

***Abstract*—X-ray Computed Tomography (CT) measurements are applied to combustion systems to obtain non-invasive three-dimensional temperature field measurements at high spatial resolution. X-ray attenuation measurements are obtained using a multi-zone silicon carbide Porous Media Burner (PMB) combusting a radiodense Kr-O_2-CH_4 mixture. A special beam hardening correction is designed to reduce the nonlinearity of the reconstructed krypton attenuation signal resuling from beam hardening by the burner wall. A statistical reconstruction algorithm is investigated to yield the noise reduction in the reconstruction domain. The ideal gas law is then used to estimate the temperature field using reconstructed krypton attenuation. The results demonstrated the potential of CT in obtaining quantitative, spatially resolved temperature field data within optically inaccessible porous media combustion environments.**

***Index Terms*—X-ray Computed Tomography, combustion, beam hardening correction, statistical reconstruction.**

I. Introduction

Porous Media Burners (PMBs) facilitate combustion of a gas mixture within the voids of a solid matrix, which results in combustion properties substantially different than those of a free flame. Stabilization of the flame inside the porous material leads to lower emissions, enhanced combustion stability at lean conditions, and increased burning rates [1]. Due to these characteristics, PMBs show promise as a more efficient, robust, and environmentally friendly alternative to a wide variety of conventional combustion systems. Potential applications for PMBs include surface heaters, domestic heating units, gas turbines, reformers, and afterburners in solid oxide fuel cells [2]. Traditional techniques for PMB combustion measurements are often based on pointwise diagnostics such as thermocouples and exhaust gas probes, which do not yield high-resolution volumetric visualization of internal flame structure or three-dimensional field data. Thus, we investigate the use of X-ray CT technology as an alternative experimental diagnostic that enables research into the detailed physical, chemical, and thermodynamic processes taking place within PMBs.

X-ray CT methods are increasingly being applied to fluid mechanics problems that involve optically inaccessible flow environments. Even in gas-phase phenomena, X-ray CT can be used to create 3-D quantitative datasets describing the mole fraction of krypton, a radiodense tracer gas, at energies characteristic of clinical and research scanners [3]. To increase the contrast of krypton gas, low X-ray energies (45-60 kVp) have been successfully used for imaging. However, as a result of the relatively high attenuation of the solid burner structure and the uncertain path length through the porous media, the transmitted X-ray spectra are altered; this affects the mass attenuation of the krypton in a complex fashion. This nonlinearity may cause inaccurate krypton attenuation measurements in reconstructed CT images. However, since most beam hardening correction algorithms are meant to obtain correct attenuation coefficients of primary attenuators in a scanned object (e.g. water and bone in medical applications), these algorithms are not necessarily well-suited for application to combustion systems where variations in gas-phase attenuation are of interest.

Although krypton has a high atomic number, the density of krypton gas is much lower than water and adipose. Thus, the krypton attenuation measured by CT reconstruction suffers severely from quantum noise. While one may acquire multiple scans and use averaging to improve the Signal-to-Noise Ratio (SNR), it is desirable to minimize the amount of time over which the data must be averaged to ensure steady-state measurements. In this work, we demonstrate that application of statistical reconstruction techniques that have performed well in medical contexts to reconstruction of attenuation data within gas-phase combustion. The application of these techniques show promise in SNR enhancement via noise reduction.

II. Porous Media Burner

The PMB investigated in this work is illustrated in Fig. 1(a). It is placed on the tabletop X-ray radiography system shown in Fig. 1(b). The burner casing consisted of a quartz tube of 0.41 cm thickness, 5.59 cm inner diameter, and 17.78 cm length. The burner matrix consistes of three adjacently placed Silicon Carbide (SiC) disks of 2.54 cm in height and 5.08 cm in diameter. A fine-pore 100 Pores-Per-Inch (PPI) disk was placed furthest upstream for use as a flashback arrestor and flow homogenizer, followed by a 65 PPI disk for flame quenching and a 3 PPI disk that functions as the combustion zone. SiC-disks were held in place via a compression fit using a ceramic fiber insulation lining, visible in Fig. 1(a).

III. Methods

A. Relation between attenuation and temperature

X-ray CT allows reconstruction of the attenuation coefficients, μ, in three spatial dimensions from a set of projections taken over a large number of angles [4]. The attenuation

M. Wu, W. Hinshaw, N. Pelc, and R. Fahrig are in the Department of Radiology, Stanford University, USA e-mail:mengwu@stanford.edu.

J. Dunnmon, and M. Ihme are in the Department of Mechanical Engineering, Stanford University, USA.

Y. Xia and A. Maier are with the Pattern Recognition Lab, Friedrich-Alexander University of Erlangen-Nuremberg, Germany.

This work is supported by the Leading Edge Aeronautic Research for Nasa (LERARN) project with award No. NNX15AE42A.

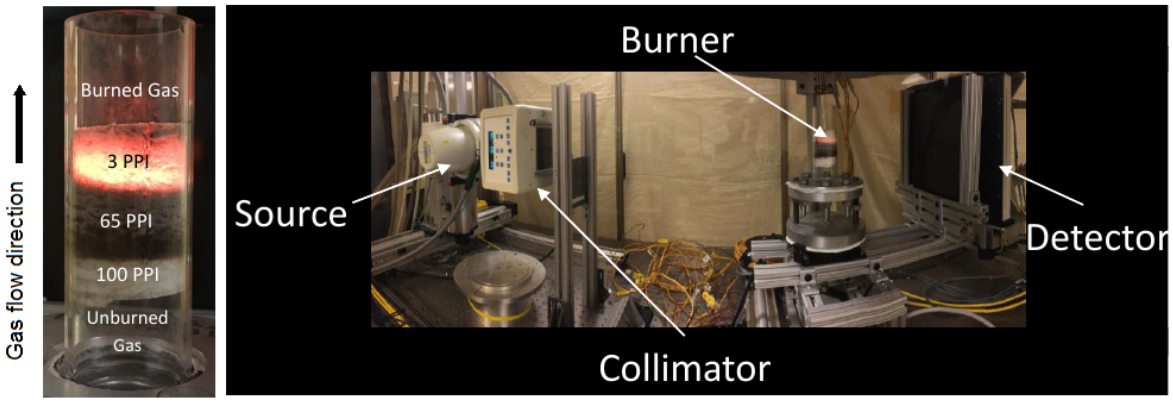

(a) Burner (b) Full Setup

Fig. 1: Experimental setup.

coefficient may be expressed as the following combination of the mass attenuation coefficient m and the density ρ of a known material,

$$\mu(\xi) = m(\xi)\rho, \tag{1}$$

where m is a nonlinear function of the photon energy (ξ) that varies with material composition. Writing Eq. (1) for a mixture of gases and introducing the partial density ρ_j gives [3],

$$\mu(\xi) = \sum_{j=1}^{N} m_j(\xi)\rho_j = \frac{P}{R_u T}\sum_{j=1}^{N} m_j(\xi)X_j W_j, \tag{2}$$

taking W_j as the molar mass of species j, R_u as the universal gas constant, and X_j as the mole fraction. In the case of a radiodense tracer gas such as krypton combined with low-attenuation gases, one may treat Eq. (2) as the combination of attenuation from the tracer and from the solid burner. In this case, one may extend Eq. (2) to yield the following simple expression for gas temperature in terms of known and measured quantities [3],

$$T = \frac{PW_{Kr}X_{Kr}m_{Kr}}{R_u \Delta\mu}, \tag{3}$$

where $\Delta\mu = \mu_M - \mu_B$, μ_B is the attenuation measured in a background scan (with only non-attenuating species in the burner), μ_M is the attenuation of the burner containing a krypton-augmented gas mixture at the effective X-ray energy, and m_{Kr} is the mass attenuation coefficient of krypton at the effective energy. Because light gases such as combustion products and ambient air attenuate negligibly at these energies, the μ_B-value is a good measurement of the appropriate signal to be subtracted to isolate the attenuation resulting from the radiodense tracer [3]. In the current work, we have used projection-based subtraction to compute $\Delta\mu$, which simplifies averaging over multiple scans while requiring only a single application of the beam hardening correction to the final projection set.

B. Beam-hardening correction

As mentioned above, the goal of the beam hardening correction presented here is different from that in most medical CT-applications. To obtain an accurate krypton attenuation image for transformation to an implied temperature signal, it is necessary to compensate for nonlinear effects of varying path length within the quartz tube and SiC porous reticulated foam that make up the body of the burner. Since subtraction is performed in the projection domain, we may apply the same correction to the background and mixture scan sets before subtraction. Note that the effect of the beam hardening correction for the quartz tube will cancel out in the subtraction process. We propose to use a two-step beam hardening correction with prior reconstruction to accurately model the effects of the two materials.

The subtracted polychromatic line-integrals of the background scan and mixture scan are:

$$\begin{aligned}\Delta y =& y_M - y_B \\ =& \log\left(\int I_0(\xi)e^{-\mu_{SiO_2}(\xi)l_{SiO_2}-\mu_{SiC}(\xi)l_{SiC}}\mathrm{d}\xi\right) \\ &- \log\left(\int I_0(\xi)e^{-\mu_{Kr}(\xi)l_{Kr}-\mu_{SiO_2}(\xi)l_{SiO_2}-\mu_{SiC}(\xi)l_{SiC}}\mathrm{d}\xi\right)\end{aligned} \tag{4}$$

where $\mu_i(\xi)$ are the attenuation coefficients of three materials, quartz, SiC, and krypton; l_i, are the path lengths, and $I(\xi)$ denotes the spectrum of the X-ray beam. The desired beam hardening gain correction for krypton is,

$$\alpha(l_{SiO_2}, l_{SiC}) = \frac{\Delta y}{\mu_{Kr} l_{Kr}}, \tag{5}$$

which is a function of path lengths in both the quartz tube and porous media. We have ignored the effect of krypton because of its very low attenuation relative to the solid, and the path length of the quartz tube can be easily calculated from a prior reconstruction. However, the path length within the porous media is hard to quantify explicitly because of its complex internal structure. We therefore simplify the process of computing the gain correction as a polynomial function of l_{SiO_2} and total line integral that includes both materials,

$$\begin{aligned}\alpha(l_{SiO_2}, l_{SiC}) &\approx \alpha(l_{SiO_2}, y) \\ &= \beta_0 + \beta_1 y + \beta_2 y^2 + \beta_3 l_{SiO_2} + \beta_4 y \cdot l_{SiO_2}.\end{aligned} \tag{6}$$

The β-coefficients can be computed with a linear fitting using known X-ray spectrum information. An example of calculated polynomial coefficient values for a 60 kVp spectrum with an

TABLE I: An example of calculated values for polynomial coefficients of the beam hardening correction for 60 kVp spectrum.

β_0	β_1	β_2	β_3	β_4
0.9528	0.1130	-0.0085	-0.0114	0.0016

effective energy of 44.8 keV is shown in Table I. For larger total line integral values, we increase the gain α to compensate for the beam hardening effect. Further, longer quartz-tube path lengths will decrease the correction gain because SiO_2 has a relatively small photoelectric effect compared to SiC. The line integral difference $\Delta y_{\text{corr}} = \alpha \cdot \Delta y$ that has been corrected for beam hardening is used during the reconstruction process.

C. Statistical reconstruction

Attenuation measurements for the krypton tracer within the reconstruction suffer from low signal–this is particularly true when the flame temperature is high. Because CT noise remains at the same level as it would in medical applications, this variation may substantially alter computed krypton attenuation in common FDK reconstructions [5]. Statistical iterative reconstruction techniques based on accurate physical noise modeling and geometric system description, on the other hand, have demonstrated significant image quality improvement over conventional methods [6]. In this study, we therefore consider the penalized weighted least-squares (PWLS) algorithm for X-ray CT reconstruction as an alternative to analytic methods. In PWLS, the attenuation field is reconstructed as,

$$\mu = \underset{0 \le \mu \le \mu_{\max}}{\operatorname{argmin}} \sum_{i=1}^{I} w_i([\mathbf{A}\mu]_i - \Delta\bar{y}_i)^2 + \beta \mathrm{R}(\mu), \qquad (7)$$

where $\mathbf{A}$ denotes the system matrix for the data acquisition geometry, Δy denotes the subtracted projection with beam hardening correction, and w contains the least-squares weights. We selected the total variation as the penalty function $\mathbf{R}$:

$$\mathrm{R}(\mu) = \sum_{j=1}^{J} \sum_{k \in N_j} |\mu_j - \mu_k|, \qquad (8)$$

where N_j denotes the indices of the neighbors of voxel j. Total variation minimization has been known to perform well in terms of both noise reduction and edge preservation. Because the quartz tube and porous media will appear as zeros in the reconstruction of subtracted projections (assuming perfect registration), we reduced the weights of the penalty function at voxels describing the solid-gas boundary by half.

IV. Experiments

All experiments were performed using the PMB shown in Fig. 1(a) on the tabletop X-ray radiography system (see Fig. 1(b)). The configuration of the PMB is detailed in Section II. The tabletop system includes a fluoroscopic X-ray source and a flat panel detector with pixel spacing of 0.336 mm. As shown in Fig. 1(b), the burner is placed between the source-collimator assembly (left) and detector (right) on a precision rotating table to acquire 1200 projections over 360 degrees.

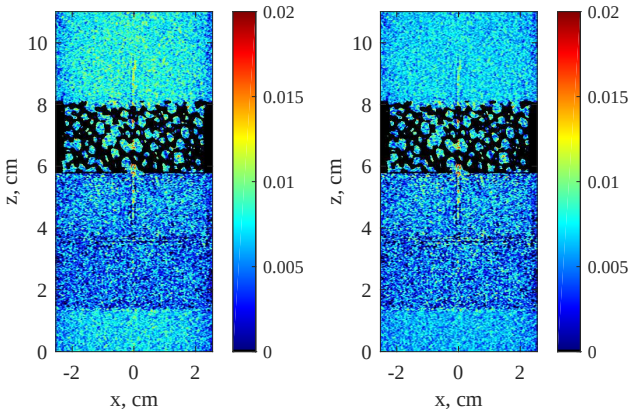

(a) Conventional correction (b) Proposed correction

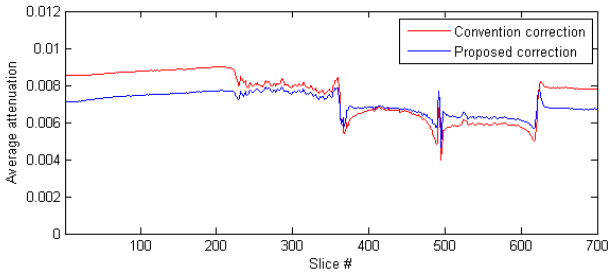

(c) Average voxel attenuation

Fig. 2: Beam hardening correction results using non-reacting scan data with cold-flow krypton concentration of 35.58% (solid mask in black).

The source-to-isocenter distance was 1061.2 mm, and source-to-detector distance was measured at 1477.9 mm. Tomographic acquisitions were conducted with a 60 kVp and 50 mA X-ray beam to optimize SNR. The 3-D reconstruction volume has a size of 384×384×700 pixels with 0.2 mm isotropic spacing.

V. Results

A. Beam hardening correction

Figure 2(a) and (b) show FDK [5] reconstructions of a tube filled with 36% krypton gas using the dual-material polynomial beam hardening correction [7] and our proposed approach. With our proposed beam hardening correction, the krypton attenuation is more uniform than with the traditional method. For instance, the differences between the gas region and porous media region are smaller than using the conventional correction—this can be observed in Fig. 2(c), which shows the cross-sectionally average attenuation coefficient of the gas voxels at different slices. With our proposed beam hardening correction approach, the reconstruction has the same krypton density inside and outside the 3 PPI porous media, while with the conventional approach this is not the case.

B. Statistical reconstruction

Reconstruction results of a PMB burning a mixture containing 82.5% krypton using both FDK and PWLS are shown in Fig. 3. We used the ADMM accelerated separable quadratic surrogate method with 30 iterations to achieve the solution of the PWLS problem for every fixed β value [8]. Even though

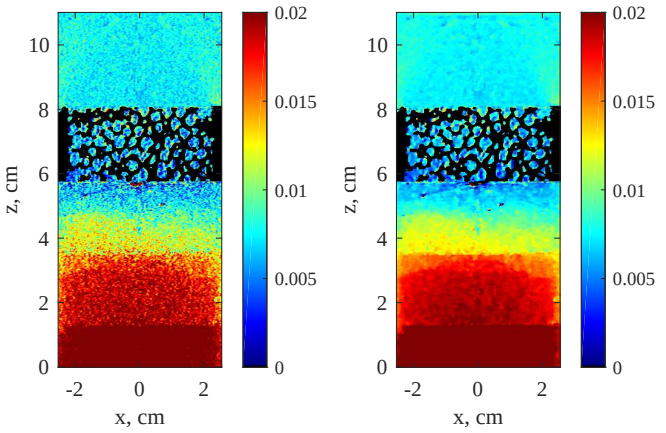

(a) FDK (b) PWLS

Fig. 3: FDK (left) vs. PWLS (right) reconstruction results using burn scan data with the krypton concentration of 82.4% (solid mask in black).

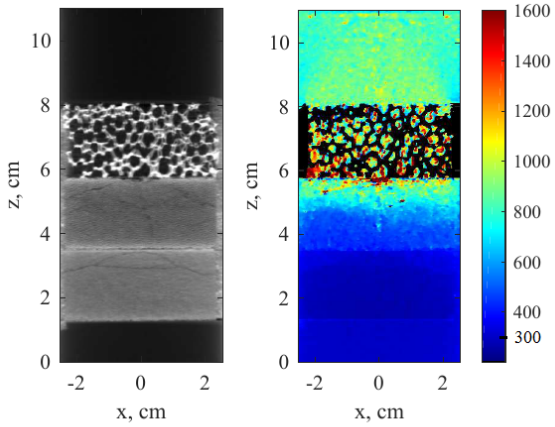

(a) Solid structure (b) Implied temperature

Fig. 4: (Left) Reconstruction result of air scan (i.e., without subtraction) to show the solid porous media structure and (right) implied temperature distribution computed from the reconstruction of PWLS (solid mask in black).

a Hamming window is applied on the ramp filtering of the FDK method to suppress high frequency components, it can be observed that the noise level is fairly high throughout the image. In contrast, the noise in the reconstruction results from the PWLS-algorithm using TV penalty function ($\beta = 4$) is substantially reduced. The interface between the different porous media sections is also more clearly visible in the PWLS result.

Finally, measured standard deviation of a homogeneous region from one reconstructed slice was substantially lower for PWLS (6.1×10^{-4}) than for FDK (2×10^{-3}), indicating that local variations present in the FDK reconstruction has been reduced by over 50 % by the PWLS technique.

C. Temperature analysis

At this point, we can use Eq. (3) to estimate an implied temperature field from the attenuation data of Fig. 3. Specifically, we estimate the temperature field by observing that the product μT is constant for constant P and X_{Kr}; this implies that temperature at a given point is simply $T = \mu_o T_o/\mu$, with inlet temperature T_o known and the attenuation values μ and μ_o obtained from the reconstruction. Note that while the 3 PPI porous media structure can be easily identified and segmented in the CT reconstruction, the 65 PPI and 100 PPI porous media is below the resolution of the CT system. We treat voxels in the 3 PPI section as the separate SiC and gas, and voxels in the 65 PPI and 100 PPI as the mixture of SiC and gas. Thus, the volume fraction of the SiC in the mixture voxels needed to be properly accounted for before converting to temperature.

Because the attenuation is in the denominator of Eq. (3), noise in this field will cause an inordinate amount of variability in the implied temperature field. Thus, reduction in krypton attenuation noise resultant from PWLS results in a substantially smoother temperature field, as shown in Fig. 4. Such results show promise in allowing for reliable extraction of 3-D flame structure and temperature fields from the PMB interior. In these images, for instance, the flame (indicated by regions of high temperature) is settled near the interface between the 3 PPI and 65 PPI regions. Substantial internal structure can be observed throughout, while heat recirculation within the solid matrix is also well visualized.

VI. Conclusion

In this paper, we have demonstrated the application of X-ray CT to combustion systems to obtain non-invasive 3D temperature field measurements. With the particularly designed experimental setup, the implied gas-phase temperature information can be derived from the 3-D reconstructed attenuation data. Further reconstruction methods are undertaken to improve the image quality, including the newly proposed beam hardening correction for reducing nonlinearity of Krypton attenuation as well as the adoption of the statistical reconstruction algorithm for suppressing the noise. From final 3D implied temperature measurements, several key internal physical phenomena, such as heat recirculation and spatial inhomogeneities within the reaction zone, can be observed.

References

[1] D. Trimis and F. Durst, "Combustion in a porous medium-advances and applications," *Combust. Sci. Technol.*, vol. 121, no. 1-6, pp. 153–168, 1996.

[2] M. A. Mujeebu, M. Z. Abdullah, M. A. Bakar, A. Mohamad, R. Muhad, and M. Abdullah, "Combustion in porous media and its applications–a comprehensive survey," *J. Environ. Manage.*, vol. 90, no. 8, pp. 2287–2312, 2009.

[3] J. Dunnmon, S. Sobhani, T. W. Kim, A. Kovscek, and M. Ihme, "Characterization of scalar mixing in dense gaseous jets using X-ray computed tomography," *Exp. Fluids*, vol. 56, p. 193, 2015.

[4] J. Hsieh, *Computed Tomography, Second Edition*. 1000 20th Street, Bellingham, WA 98227-0010 USA: SPIE, Oct. 2009.

[5] L. Feldkamp, L. Davis, and J. Kress, "Practical cone-beam algorithm," *J. Opt. Soc. Am. A*, vol. 1, no. 6, pp. 612–619, 1984.

[6] J.-B. Thibault, K. D. Sauer, C. A. Bouman, and J. Hsieh, "A three-dimensional statistical approach to improved image quality for multislice helical CT," *Med. Phys.*, vol. 34, no. 11, p. 4526, 2007.

[7] J. Hsieh, R. C. Molthen, C. a. Dawson, and R. H. Johnson, "An iterative approach to the beam hardening correction in cone beam CT.," *Med. Phys.*, vol. 27, pp. 23–9, Jan. 2000.

[8] H. Nien and J. A. Fessler, "Fast X-ray CT image reconstruction using the linearized augmented Lagrangian method with ordered subsets," *arXiv Prepr. arXiv1402.4381*, p. 21, Feb. 2014.